Ultrasonics Sonochemistry 73 (2021) 105520

Contents lists available at ScienceDirect

Ultrasonics Sonochemistry

journal homepage: www.elsevier.com/locate/ultson

Cavitation-assisted decontamination of yttria from graphite of different densities

S. Lahiri [a,b,*], D. Mandal [b,c], P.R. Gogate [d], A. Ghosh [e], R.L. Bhardwaj [a]

[a] Laser & Plasma Technology Division, Bhabha Atomic Research Centre, Mumbai 400085, India
[b] Homi Bhabha National Institute, Anushaktinagar, Trombay, Mumbai 400094, India
[c] Alkali Material & Metal Division, Bhabha Atomic Research Centre, Trombay, Mumbai, 400085, India
[d] Institute of Chemical Technology, Matunga, Mumbai 400019, India
[e] Glass & Advanced Materials Division, Bhabha Atomic Research Centre, Trombay, Mumbai 400085, India

ARTICLE INFO

Keywords:
Yttria
Graphite
Cavitation
Ultrasound
Process intensification

ABSTRACT

Yttria coated graphite crucibles are widely used to handle molten refractory and radioactive metals like uranium and plutonium. However, the coated layer suffers damages like cracking and peeling off owing to thermal cycles. As a result, removal of the yttria layer from the graphite surface is essential to ensure reuse of the crucible and minimization of radioactive waste. The present work investigates intensified dissolution of yttria from the coated graphite samples using ultrasound as a non-destructive decontamination technique to recycle the graphite substrate. The optimum conditions established for maximum dissolution were 8 M as acid strength, frequency of 30 kHz, temperature of 45 °C and power density of 8 W cm^{-2} that resulted in maximum dissolution of 52% in 30 min. Use of an oxidant H_2O_2 to the acid, did not yield any improvement in the dissolution kinetics, instead, increased oxidation of the graphite substrate was observed, leading to the anomalous weight gain of the graphite substrate despite surface erosion. Effect of ultrasound on the dissolution was pronounced, with almost a threefold increase compared to dissolution performed under silent conditions. Rates of dissolution of yttria from the substrate of different densities and pore size distribution were also studied. The dissolution was slowest from graphite of density 1.82 g cm^{-3} as the pore size distribution was conducive to accommodate the yttria particles. The dissolution in nitric acid followed ash layer diffusion controlled kinetics. The study has demonstrated the efficacy of application of ultrasound for accelerated decontamination of graphite substrates.

1. Introduction

High-density graphite (HDG) is widely used as crucibles and substrates to handle nuclear materials *viz.*, uranium and plutonium [1–3]. It is susceptible to oxidation in atmosphere at temperatures above 500 °C, but stable at temperatures around 3000 °C in high vacuum [4–6]. A protective coating on graphite prevents the unwanted chemical interaction between molten metal and carbon, and thus ensures high corrosion resistance and longer service life at the desired operating temperature. The coating also prevents deposition of molten metal on the porous surface. Yttria (Y_2O_3) is widely used as a high temperature coating material on the graphite for nuclear applications. Y_2O_3 provides a stable and non-interacting coating on graphite with effective use till temperature of 1600 °C [7,8]. However, difference in the thermal expansion coefficient (TEC) between HDG and Y_2O_3 causes formation of cracks in the top-coat. Residual oxygen diffuses through the cracks and oxidizes the carbon. Formation of non-stoichiometric oxide of yttrium during prolonged exposure of the coating at a temperature above 1400 °C would release oxygen, which can also enhance the oxidation of graphite. This phenomenon of partial oxidation spreads laterally at the HDG-Y_2O_3 interface. The top Y_2O_3 delaminates locally when two such pockets meet [9]. Considering the observed effects over prolonged use, removal of residual yttria coating from graphite is typically essential, before any reuse can be thought about. The effective stability of coating is seen for a few (around 10) thermal cycles at 1500 °C. For any reuse of the material based on the recoating of the yttria on the graphite crucible or substrate, it is important that the previous damaged layer is removed. Currently acid leaching is the commonly applied method, though it is not efficient process due to slowness and it cannot remove material completely from pores. Therefore, developing technique to hasten

* Corresponding author.
E-mail address: sutanwi@barc.gov.in (S. Lahiri).

https://doi.org/10.1016/j.ultsonch.2021.105520
Received 28 December 2020; Received in revised form 1 February 2021; Accepted 8 March 2021
Available online 14 March 2021

dissolution, both from the surface and pores is of utmost importance.

Ultrasound offers a useful process intensification alternative, especially for the porous substrates, as showed for uranium in our earlier work [10]. In the case study with uranium, Physical Vapour Deposition (PVD) technique was used to coat the graphite coupons. In the subsequent dissolution studies, maximum dissolution of uranium deposits was reported at optimum conditions of 1.2 W cm^{-2} as the power density and 33 kHz as the operating frequency. Moreover, the study revealed a two-fold increase in dissolution rate due to sonication. During ultrasonic treatment, cavity formation takes place in the liquid medium. This acts as a high temperature high pressure micro scale reactor, yielding higher dissolution rates. Besides, the radical formation in the bubbles intensifies the chemical reactivity. Bursting of the cavitation bubbles on the surface of the substrates and inside pores dislodges material embedded in them and enhances mass transfer rates by microstreaming [11]. In addition to the demonstrated effect for the uranium dissolution, ultrasound has also been effectively harnessed for process intensification in hydrometallurgical applications for the leaching of ores of copper [12], nickel [13], and uranium [14,15]. It is important to note that no study reported the application of ultrasound for intensification of dissolution of yttria. Earlier studies have reported yttria removal by using solvents, for example, alkaline leaching of yttria from eutectic superalloy in autoclaves [16] and recovery of yttria from rare earths [17]. Dissolution of yttria in autoclaves entails use of high pressures as high as 85 atm [16] and temperature as high as 150 °C [17]. Such extreme process condition is useful in hydrometallurgy. However in the case of decontamination processes, use of high pressure and temperature will also lead to the disintegration of the substrate (graphite). Therefore, the chances of recycling the graphite would be reduced and a lot of carbon residue might be generated which would require further processing. A low temperature and pressure process is conducive for decontamination and the present work attempts to develop such process based on the use of ultrasound.

The novelty of the present work lies in demonstrating the use of ultrasound for yttria dissolution from the graphite surface and pores at lower temperature and pressure compared to conventional autoclave leaching. The work also demonstrates understanding into effect of concentration of acid, reaction temperature, operating frequency and power density of the ultrasound on the dissolution process and its kinetics. Effect of adding oxidant on the kinetics was also studied along with the influence of pore size distribution for graphite of different densities. The outcome of the work is important as this will not only bring down the volume of graphite wastes generated by the nuclear installations, but also to bring down the radiological exposures and environmental pollution caused by its burning.

2. Materials and methods

2.1. Materials and sample preparation

In order to study the dissolution of yttria in dilute nitric acid, yttria slurry (from M/s Indian Rare Earth Limited) was coated on the graphite tokens, after degassing them in a vacuum furnace at 1200 °C to release all trapped gases and hydrocarbons [18]. For Y_2O_3 coating, a slurry of yttria nanoparticles was prepared in aqueous medium using polyacrylic acid (PAA with 2000 as molecular weight, Aldrich) and 2 wt% of dry weight of Y_2O_3 at pH of 9.0 in a planetary mill (Fritsch, Germany) operated at 120 RPM. Zirconia pot and ball were used for ensuring required mixing. The size of the yttria nanoparticles varied between 90 and 120 Á. Weight ratio of yttria and water in the initial slurry was 75:25. Subsequently, the slurry was diluted to 50:50 as Y_2O_3 to water weight ratio. This slurry was applied on graphite by paintbrush method. The test coupons were heated to 400 °C at a heating rate of 60 °C h^{-1}. After holding for 30 min, the coupons were heated to 800 °C at a heating rate of 90 °C h^{-1}.

The coupons for the leaching test were obtained by depositing a 200 μm thickness layer of yttria on graphite of density 1.82 g cm^{-3}. The diameter of the tokens is 18 ± 0.5 mm. The initial weight of the uncoated graphite token is 4300 ± 40 mg whereas the weight of the yttria deposit was 82 ± 0.1 mg.

In order to test the effect of pore size distribution on the dissolution process, graphite of different densities were tested. Mercury porosimetry tests (using Thermo Fisher Scientific Mercury Porosimeter – Pascal Series) were conducted to determine the pore size distribution and specific surface areas of the graphite of different densities. The particle size distribution of yttria was determined using Mastersizer 2000 (M/s Malvern Panalytical). An environmental scanning electron microscope (Quanta 200 ESEM, FEI, USA) was also used to characterize the microstructure of the graphite substrate before ultrasonic treatment and after ultrasonic treatment to study the effect of using ultrasound on erosion.

2.2. Leach solutions and experimental setup

The leach solutions of 15 ml volume were prepared with nitric acid (HNO_3) at different concentrations. Since the work mainly targeted at decontamination of yttria coated graphite crucibles that mainly process molten uranium and plutonium, nitric acid is considered as the best choice for the leachant. Rao *et al.* confirmed the percolation of liquid uranium through microcracks during the peeling off of the yttria top coat and hence contaminated crucible may have uranium embedded in the yttria layer as well [10]. Yttria is soluble in molten uranium around 1400 °C, as also reported by Condon et al. [21].

Ultrasound irradiations at different frequencies as 20 ± 2, 30 ± 3 and 40 ± 3 kHz were employed using a 1.5 L in-house built ultrasonic cleaning bath, having dimensions of height, width and depth as 240 mm × 140 mm × 60 mm, respectively. Two transducers (M/s Morgan Matrac make) of size 2″each, were screwed to the base of the tank from the outer side. Each beaker, containing the test solution and mounted on a metal basket, was dipped in the bath. A schematic of the experimental setup is given in Fig. 1. Generally, the acoustic intensity was maintained at 8 W cm^{-2} in all experiments (except the ones described in Section 3.5 related to the variation in the acoustic intensity over the range of 1 and 10 W cm^{-2}). Around 10 mm distance between the bottom of the beaker used as reactor and the bottom of the ultrasonic bath was maintained. The ultrasonic bath was filled with demineralised water upto a level of 30 mm to provide a medium for sonication and the temperature was measured by digital controller with a PT100 sensor. The bath was placed in a fume-hood to route the NOx fumes generated to the surroundings after suitable dilution with air. The temperature of the bath was maintained at 45 ± 3 °C, except in studies related to understanding the effect of variation in temperature. The bath is provided with a variable input power supply to the two transducers available at the bottom of the ultrasonic bath. The total combined power to the two transducers is in the range 0 to 100 W as varied using the controller available with the unit. The input power was varied over the described range to test the efficacy of ultrasound in the dissolution process. The diameter of the two transducers mounted on the bottom face is 2.5 cm each and hence the

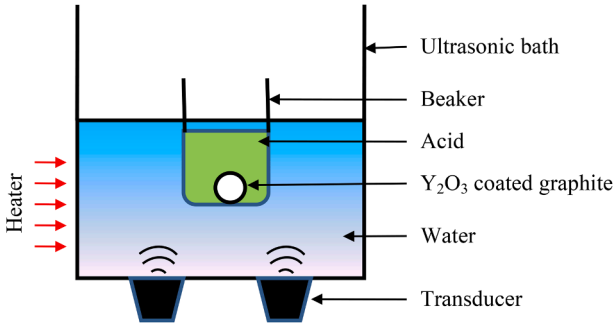

Fig. 1. Typical experimental setup for leaching using ultrasonic bath.

acoustic intensity range applied in the present work is 0 to 10 W cm^{-2}.

2.3. Analysis of leach liquor samples

The leachant samples were withdrawn at equal intervals of time. The carbon dust was filtered using a 500 μm Whattman paper and the supernatant liquid samples containing dissolved yttrium was analysed for the yttrium content in Inductively Coupled Plasma-Optical Emission spectrophotometer (ICPOES). The residue obtained in filtration was analyzed using Fourier Transform Infrared Spectrometer over the wavelength range of 4000 to 500 cm^{-1} (M/s Bruker Vertex 70 V) to determine the change in the functional groups on the carbon after exfoliation.

2.4. Weighing precision and statistical analysis

The weight of the graphite sample before and after the experiments was measured using the Afcoset HR-250 AZ weighing balance, having readability till 0.1 mg. The weighing was done thrice and the average value is reported. All the experiments/measurements were carried out as duplicates of at least 2 and the average value was reported. In the case of a large variation, the experiments were repeated afresh and the average value of all the measurements reported. The errors in the measurements have been depicted in terms of error bars in the graphical representation and the typical variation was in the range of ±2% of the reported average values. For the kinetic models, model parameters were fitted with non-linear regression using Origin 6.0. The coefficient of determination (R^2) is a measure of goodness of fit for linear models and applied in the work to establish the effective fitting of the models.

3. Results and discussion

3.1. Analysis of the graphite coupons used

Extruded graphite from M/s Graphite (India) Limited, having density of 1.82 g cm^{-3} and 18% porosity, was used as a substrate (except in the study relating to variation of pore size distribution, where densities 1.6 g cm^{-3} and 1.92 g cm^{-3} were also explored).

A typical graphite sample, coated with yttria is shown in Fig. 2(a). The peeling of yttria coating after a number of thermal cycles is demonstrated in Fig. 2(b). It can be clearly seen that the top coat has come off due to the difference in the thermal expansion coefficients of the coating and substrate. In the case of graphite crucibles processing uranium or other refractory metals, such delamination occurs in much less thermal cycles [9] and hence the surface needs to be reprocessed. The slurry coated graphite tokens were sonochemically treated in acid and the leach liquor was taken out for analysis after a certain period. Fig. 2(c) shows a leach liquor sample, obtained immediately after sonication. On standing for more than 6 h, sedimentation of the suspended particles leaves a supernatant at the top, which is then sent for ICPOES analysis, after suitable filtration.

The micrographs of the graphite surface before deposition of the coating and after removal of the yttria layer, are given in Fig. 3a-c. The surface morphology of the as-received graphite surface, cleaned with emery paper, is shown in Fig. 3(a). Fig. 3(b) of the coated graphite surface shows a fairly uniform yttria coating. The graphite surface shows the presence of macroporous opening (Fig. 3(c)) after the ultrasound treatment similar to that observed in the case of uranium leaching [10] under similar conditions (30 kHz as frequency and 30 min as the time of treatment). However, the degree of pore opening in the case of yttria coating was less compared to that of uranium. The molten uranium

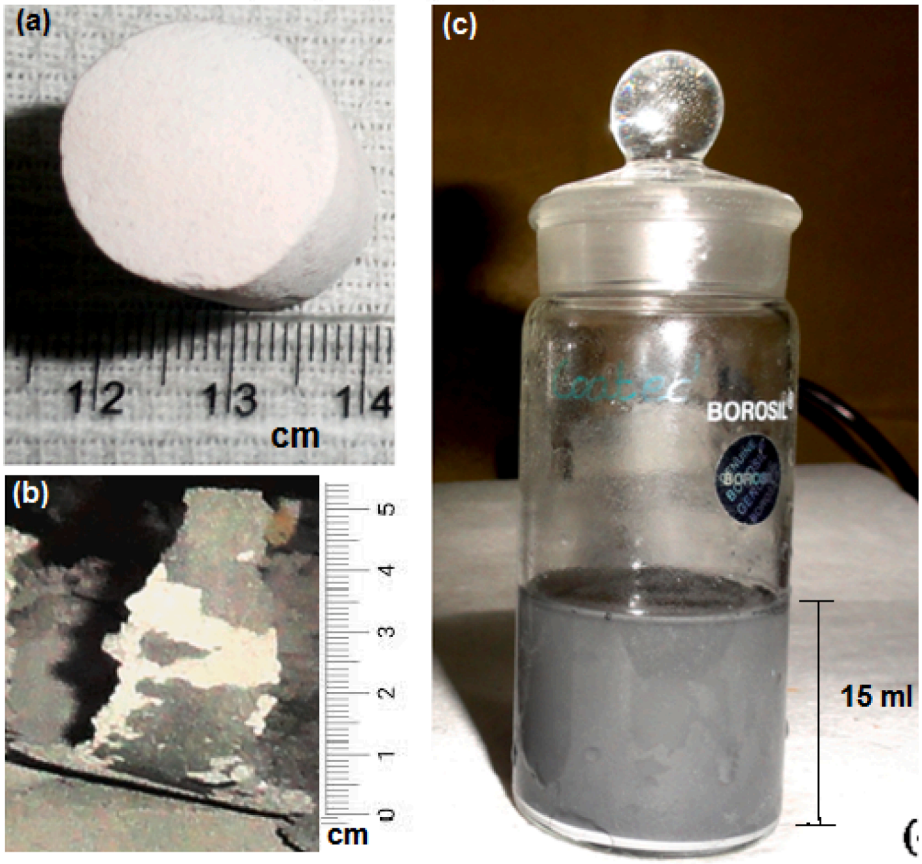

Fig. 2. (a) Slurry coated yttria on a graphite piece, (b) Yttria coating peeling from graphite substrate, (c) Sample containing yttria dissolved in nitric acid (immediately after sonication).

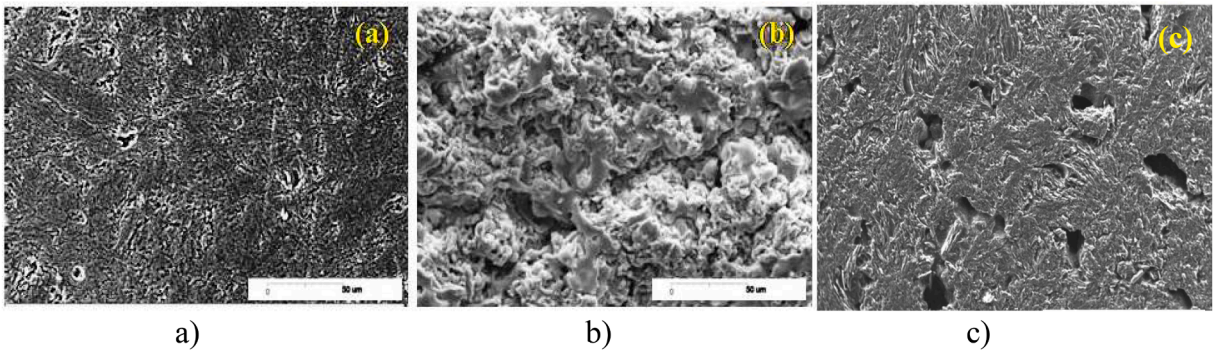

Fig. 3. SEM micrographs of (a) graphite surface before coating (b) yttria coating (c) graphite surface after yttria recovery at 30 kHz for 30 min.

deposited by physical vapour deposition (PVD) on graphite electrodes forms a stronger bond with graphite. This is due to the Van der Waals forces, and electrostatic attraction between substrate and coating in sputter coating [19]. The uranium deposit diffuses deeper into the pores and acid leaching inside these pores leads to further pore opening due to removal of uranium to higher extent. The weaker mechanical bond formed by slurry coating between the graphite surface and yttria could be easily overcome by cavitation. The technique used to coat surface plays a role in the extent of leaching and subsequent morphology of the substrate, thus different observations are made for the case of uranium

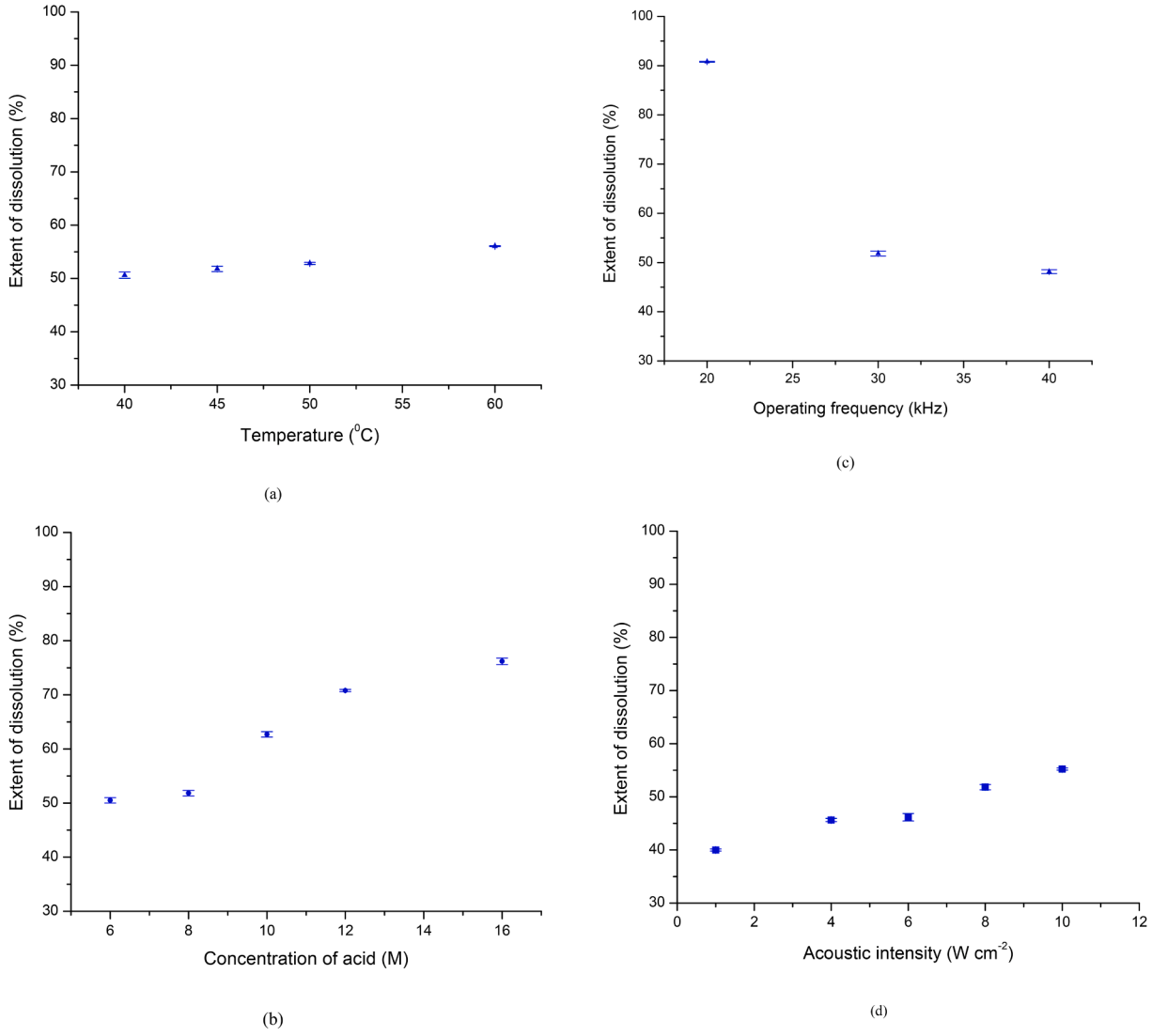

Fig. 4. (a) Effect of temperature on the extent of dissolution (using 8 M HNO_3 solution under 30 ± 3 kHz ultrasonic field with an acoustic intensity 8 W cm^{-2}), (b) Effect of concentration of acid on the extent of dissolution (under 30 ± 3 kHz ultrasonic field with an acoustic intensity 8 W cm^{-2}), (c) Effect of operating frequency on the extent of dissolution (using 8 M HNO_3 solution with an acoustic intensity 8 W cm^{-2}), (d) Effect of acoustic intensity on the extent of dissolution (using 8 M HNO_3 solution under 30 ± 3 kHz ultrasonic field).

and yttrium demonstrating the importance of the work.

The Energy Dispersive X-ray (EDX) studies of the yttria coating (after heat treatment) showed presence of carbon (2% w/w) as a dispersed phase. Formation of yttrium carbide is not anticipated as yttrium oxycarbide is formed at 1700 °C and subsequently the oxygen is removed to form the monocarbide, YC in vacuum at 1900 °C. [20]

3.2. Effect of temperature on the extent of dissolution

The experiments were performed using 8M HNO_3 solution under 30 ± 3 kHz ultrasonic field with an acoustic intensity of 8 W cm^{-2} (80 W power) applied for 30 min. The varying reaction temperatures were selected over the range of 40 °C to 60 °C. Temperature beyond 60 °C was not explored in the present work due to the limitations of glued Lead Zirconate Titanate (PZT) transducers.

The effect of temperature on the dissolution of yttrium is illustrated in Fig. 4(a). The maximum amount of yttrium that can be dissolved in the 15 ml acid solution was 4100 ± 40 ppm, as calculated from the weight of the deposit. The results demonstrated in Fig. 4(a) established that the dissolution rate increased with an increase in temperature of the acid leachant. Quantitatively, the dissolution of yttrium in acid increased from 50% (2050 ppm) to 55.4% (2270 ppm) of the total weight of the deposit (4100 ± 40 ppm) with an increase in temperature of the leachant solution from 40 °C to 60 °C (as seen in Fig. 4(a)). Dissolution % mentioned in the results is the ratio of the amount of yttrium dissolved in a particular scenario to the total amount of yttrium in the coating expressed as %. A rise in temperature leads to enhanced sonolysis of water and acid, decrease in viscosity and surface tension along with an increase in the vapour pressure of the solvent (acid). Therefore, cavitation bubbles are generated easily at higher temperatures, leading to faster dissolution. Increase in temperature also favors the kinetics of reaction leading to higher recovery. Such instances were also observed in the case of delignification of newspaper where the extent of treatment enhanced from 16% to 44% by increasing the temperature from 40 °C to 100 °C [22]. Similarly in the case of uranium, the dissolution rate changed by 20% over the temperature range of 45 °C to 70 °C for treatment of 30 min at 33 kHz frequency in 6 M acid solution [10].

It is also noted in the current work that temperature is a less sensitive parameter as the change in dissolution is only 5% over a change in temperature of 20 °C. Thermodynamically, due to the exothermic nature ($\Delta H = -ve$) of the dissolution reaction, the kinetics of the reaction is more spontaneous at higher temperature and hence the rate is expected to be higher. However, at higher temperature, a large number of bubbles formed in the liquid act as cushion and attenuate the mechanical effect of bubble implosion on the graphite surface. Therefore, an operating temperature of 45 °C may be considered optimum for the dissolution process and further parametric studies were carried out at this temperature in this work.

Around 60 °C, the evolution of visible red NO_x fumes started as observed visually. The NO_x fumes get diluted by air in the fume hood and are discharged to the atmosphere at concentration levels < 1 ppm. The current ACGIH recommendation is for a 3 ppm time weighted average (TWA) and a 5 ppm as the short term exposure limit (STEL). The work was carried out on small samples having around 82 mg yttria. In the case of scale-up, a higher acid concentration and an increased dissolution rate will lead to a higher rate of NOx generation. This might easily breach the TWA values specified by ACGIH or the threshold values set by local regulatory bodies. High flux of NOx was also observed to cause pitting on the SS-304 ducts. So, a lower operating temperature as compared to the maximum investigated is being recommended as optimum considering counteracting phenomena of enhanced dissolution and higher pitting/generation of NOx gases.

3.3. Effect of the HNO_3 concentration on the extent of dissolution

The plots of the extent of dissolution at different concentrations of HNO_3 under 30 kHz ultrasonic field, are given in Fig. 4(b). Nitric acid is a strong oxidizing agent. With 8 M HNO_3, the dissolution of 50% was obtained in 30 min at 45 °C. As the concentration increases, the dissolution is favoured based on higher availability of the acid to generate radicals that initiate the reaction [10].The increase was gradual between 6 M and 8 M. It is also interesting to note that a 10% jump in dissolution is seen from 8M to 10 M acid concentration. Beyond 10 M, the increase in dissolution was around 5% for every 2 M increase in concentration, till 16 M. Overall, the trend shows that increase in acid concentration from 6 to 16 M is instrumental in almost linearly increasing the extent of dissolution by 26%, exactly similar to the trend observed in the case of uranium dissolution under similar conditions [10]. It is also important to note that significantly higher acid concentration gives rise to problems during scale-up. Nitric acid being extremely corrosive, may lead to corrosion in the welds of the ultrasonic bath. The corrosive effects are further enhanced due to the cavitation and implosion of bubbles which will help in propagating the defects. Also, the use of highly concentrated nitric acid is accompanied by the generation of NOx gases that has to be diluted to a suitable concentration as per the local environment protection guidelines before disposal. The rate of generation of NOx gases will be higher at higher strength of acid and hence it is very important to decide on optimum concentration. Pitting of the graphite substrate also cannot be ruled out at higher molarities. Based on the obtained results in the current work, it can be said that concentration of 8 M is sufficient to bring about optimum dissolution based on the thickness of the coat and minimum expected negative effects. Therefore, all the subsequent experiments in this work used 8 M acid for parametric study.

3.4. Effect of operating frequency on the extent of dissolution

The effect of different operating frequencies as 20 kHz, 30 kHz and 40 kHz were studied to understand the effect on graphite decontamination. The acoustic intensity maintained for all frequencies of operation was 8 W cm^{-2} (80 W as the net power dissipation). It was observed that dissolution at 20 kHz was almost complete (99.8%) in 30 min, whereas it was only 52% complete at 30 kHz and 48% complete at 40 kHz (Fig. 4(c)). Cavitation and subsequent implosion of bubbles on the surface on the substrate is more rigorous at lower frequencies compared to higher frequencies. At lower frequencies, the bubbles formed are larger and they render higher physical effects on the substrate to dislodge the contaminants. It can be thus concluded that the physical effects of turbulence and acoustic streaming play a major role in dislodging of deposit from the surface leading to enhanced dissolution of yttria in acid. Due to the lower physical effect with an increase in operating frequency, the extent of dissolution was lower at higher frequencies as 30 kHz and 40 kHz. The controlling mechanism of intensification is confirmed by the significant decrease in extent of dissolution by 50% by changing the operating frequency from 20 to 30 kHz, which is far more than observed with the other parameters. However, subsequently the extent of dissolution only changed marginally from 51% to 48% for a frequency change from 30 kHz to 40 kHz. A decrease in dissolution rate from 72% at 20 kHz to 51% at 33 kHz and to 36% at 40 kHz was also reported after 30 min for uranium dissolution [10]. It is important to note that though the trends are similar, the actual extent of reduction in the extent of dissolution is different directing the importance of the presented work.

It was also established in the work that use of 20 kHz frequency gives best decontamination but also leads to the erosion of the graphite surface, preventing its recycle. It was hence concluded that 30 kHz is the optimum frequency of the dissolution process as the mechanical effects of ultrasound is sufficient to bring about decontamination and also maintaining the stability of the graphite surface. Therefore, the frequency of 30 kHz was used for the parametric studies in this work.

3.5. Effect of acoustic intensity on the extent of dissolution

An important factor affecting the sonochemical effects is the amount of energy entering in the bulk of liquid as well as the area of transducers [23]. Bubble dynamics is a stronger function of power dissipation rate and hence there is a significant effect on the cavitational intensity typically described as the quantification of cavitational effects in terms of collapse temperature pulse or the degree of turbulence under the given set of operating conditions. It is expected that higher acoustic intensity will give higher cavitational intensity and hence favor the applications. In the case of reactions at a constant temperature, using too high power density, however, will necessitate higher cooling water flow requirement and a waste of energy dissipated as heat. Such heat may also cause local hotspots near the transducers thereby lowering their life as well as decoupling losses. Moreover in industrial reactors or baths, higher vibrational amplitude will lead to development of cyclic stress in the welds, leading to their failure. The optimum magnitude of power dissipation is a function of frequency of irradiation, reactor geometry, physicochemical properties of bulk liquid, location and surface area of irradiating element and the desired application; overall there is a strong need to investigate the effect of acoustic intensity for any application confirming the importance of the presented work.

As shown in Fig. 4(d), the dissolution of yttria was observed to increase monotonously from 40% to 55% as the intensity increased from 1 to 10 W cm^{-2} (100 W) in the 30 kHz frequency cavitation field at 45 °C. It is important to note that there is no optimum intensity within the tested range of power density for giving maximum effects of yttria dissolution unlike that observed in the case of uranium [10] confirming that the trends depend on the specific application and the range of acoustic intensity investigated. In the case of uranium dissolution, maxima at 1.2 W cm^{-2} for 20 kHz and at 1.5 W/cm^2 for 33 kHz were observed for a treatment time of 90 min at 70 °C with 6 M acid strength being used in the work. Typically with an increase in the acoustic intensity, the bubble formation increases leading to higher cavitational effects and hence an increase in the dissolution is observed. It is expected that for the given reactor geometry, operating temperature and frequency, the shielding effect of the bubbles and decoupling losses are not observed in the current work over the range of acoustic intensity investigated [17] giving a continuous increase in the dissolution with intensity. It is important to note that result may not be generalized and best acoustic intensity need to be established for the specific application as per method depicted in this work.

3.6. Effect of adding oxidant to the acid on the extent of dissolution

An oxidizing agent was added to the leachant acid to test the efficacy of dissolution of yttria and oxidation prospects of the substrate. Studies investigated the effects of H_2O_2 concentration on sonochemical reactions [24,25] and reports were seen beneficial based on the generation of enhanced hydroxyl radicals. It is also observed that there is formation of H_2O_2 during the sonolysis of water [26] though the quantum is not significant enough to yield any enhanced oxidation capacity and hence it may be important to use external addition of H_2O_2. The addition of 0.1 mM and 1 mM hydrogen peroxide as an oxidizing agent was not found to make any significant improvement in the dissolution process, as per the results shown in Fig. 5. Since yttrium ion has only one oxidation state +3, further increase in dissolution rate was not observed. Moreover, the hydroxyl ions generated by the sonolysis of water recombine to form H_2O_2. Based on Le-Chatelier's principle, the addition of hydrogen peroxide disrupts this recombination of hydroxyl free radicals yielding scavenging action of H_2O_2 as also reported by Lim *et al.* [27]. The hydroxyl free radicals that exist in aqueous solution were reported to be scavenged by excessive hydrogen peroxide molecules to form much less oxidative hydroperoxyl radicals. The presented results in the work clearly establish that use of oxidants is not necessarily effective in all the cases of ultrasound induced intensification. The role of ultrasound in intensifying the extent of dissolution is also clearly demonstrated based on the comparison with silent conditions and the detailed mechanistic understanding into intensification has been provided in the next section.

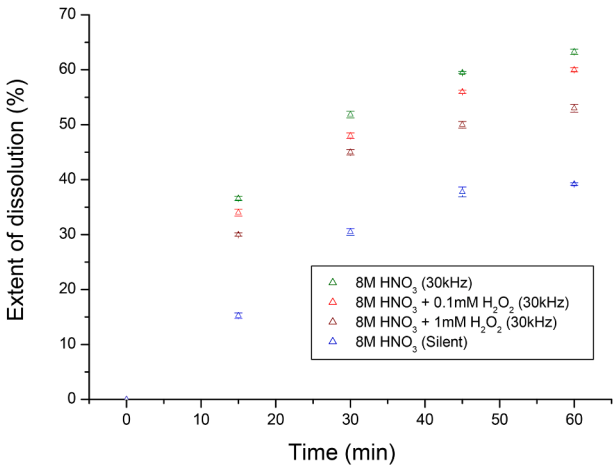

Fig. 5. Effect of adding oxidant to the leaching acid (8 M HNO_3 solution on the extent of dissolution under 30 ± 3 kHz and comparing dissolution in the absence of ultrasound.

3.7. Comparison of kinetics with and without the use of ultrasound

Fig. 5 also shows the change of dissolution of yttrium expressed in % with time in the presence and in the absence of ultrasound. The comparison was done under conditions of 40 °C temperature and 8 M HNO_3. Dissolution at an operating frequency of 30 kHz was compared with silent dissolution. The silent dissolution process reaches equilibrium at early extent of dissolution as 38%, beyond which no significant increase was observed. In the sonicated process conducted at 30 kHz and 8 W cm^{-2} power density, the extent of dissolution achieved was 60% after 45 min. The dissolution also showed an increasing trend beyond 45 min without any sign of reaching a steady state at 1 h.

In order to establish the efficacy of ultrasound in the intensification of the dissolution process using the kinetic parameters, the data on dissolution kinetics was similarly analysed for silent conditions. The rate constant of dissolution was found to be 0.066 h^{-1} for reaction conducted at 40 °C under silent conditions. At the same temperature, the rate constant in the presence of ultrasound (30 kHz) was 0.214 h^{-1}. It can be thus clearly established that when ultrasound is applied to the system, the rate constant is enhanced by a factor of 3.2, compared to that in the silent reaction, which can be attributed to the enhanced turbulence and local hot spots being generated in the system due to the cavitating conditions generated by passage of ultrasound under optimum conditions.

3.8. Weight gain of the graphite substrate after exfoliation

The decontaminated graphite samples were degassed till 1200 °C and the final weights were measured. An anomalous increase in the weight of the graphite was observed after the decontamination process despite the erosion and subsequent sedimentation of the carbon dust. The competition between the expected weight reduction due to the generation of the carbon dust and the weight increase due to the surface oxidation of the graphite played a role. The FTIR spectra (Fig. 6) of the decontaminated graphite showed the presence of peaks at 3422, 1720, 1625, 1390, 1226 cm^{-1} due to —OH stretching, C═O stretching, —OH bending, and C—OH stretching which were absent in the untreated samples [28]. This confirmed the oxidation of the surface into graphite oxide leading to weight gain of the graphite substrate despite erosion.

The addition of H_2O_2 was found to increase the oxidation of graphite,

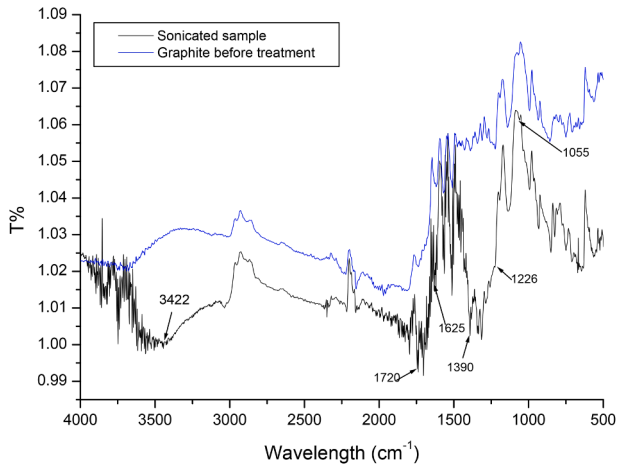

Fig. 6. FTIR spectra of fresh graphite and graphite after decontamination in 8 M HNO_3 solution at 30 ± 3 kHz frequency and with an acoustic intensity 8 W cm^{-2}.

thereby increasing the erosion rate by exfoliation. Erosion rate in both the cases (only nitric acid medium and nitric acid and hydrogen peroxide medium) was studied at the same operating frequency 20 kHz, where maximum oxidation is expected among the different applied frequencies. The increase in weight with the addition of H_2O_2 to nitric acid, as shown in Table 1, is almost ten times the increase in weight in only nitric acid medium.

A possible exfoliation mechanism based on the experimental results and published literature [29–32] is proposed. The aqueous solution of nitric acid, which contains OH^- ions, reacts with H_2O_2 to form highly nucleophilic O_2^{2-} ions [32–34], which can intercalate into graphite sheets. In the absence of H_2O_2, the low-nucleophilicity OH^- ions do not effectively intercalate and/or have poor interactions with graphite. Thus, H_2O_2 plays a crucial role in the sonochemical exfoliation of graphite.

3.9. Effect of graphite pore size distribution on the kinetics

The particle sizes of the yttria powder used for coating determine the extent to which the pores are accessible. Particle size distribution of the yttria powder, shown in Fig. 7(a), typically varied in 0.5–10 μm range. The pore size distribution of graphite of three different densities (1.6 g cm^{-3}, 1.82 g cm^{-3}, 1.92 g cm^{-3}) is shown in Fig. 7(b). The micrograph of graphite of density 1.6 g cm^{-3} (Fig. 7(c)) shows widespread defects and discontinuities compared to the microstructure of graphite of densities as 1.82 g cm^{-3} and 1.92 g cm^{-3}. The graphite with the highest density 1.92 g cm^{-3} was almost defect-free, thereby justifying the pore size distribution given in Fig. 7(b).

It was observed that the dissolution kinetics (Fig. 8) is slowest in graphite of density 1.82 g cm^{-3} while it is the fastest for the density as 1.92 g cm^{-3}. This can be explained from the fact that graphite of density as 1.82 g cm^{-3} has 68% pore volume distributed in pores of diameter

Table 1
Weight gain of graphite substrate and carbon dust generation due to erosion in different leachants (at 20 kHz, 45 °C).

Leachant	Initial weight of graphite (g)	% Weight gain of graphite	% of C dust
8 M HNO_3	1.394 ± 0.04	0.165 ± 0.02	0.23 ± 0.01
8 M HNO_3 + 0.1 mM H_2O_2	1.368 ± 0.02	1.56 ± 0.03	0.44 ± 0.01
8 M HNO_3 + 1 mM H_2O_2	1.327 ± 0.03	1.83 ± 0.02	0.53 ± 0.02

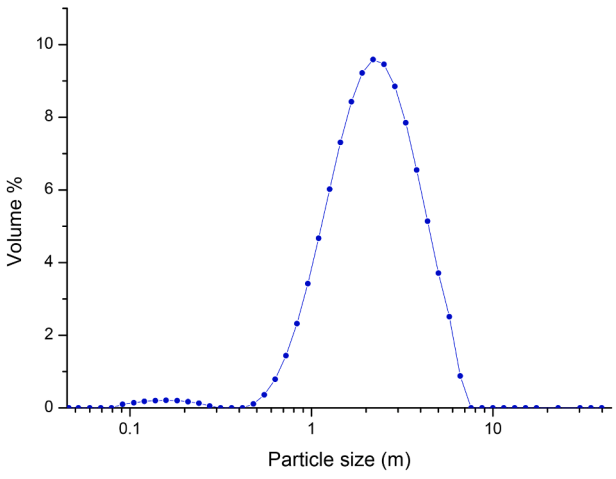

(a)

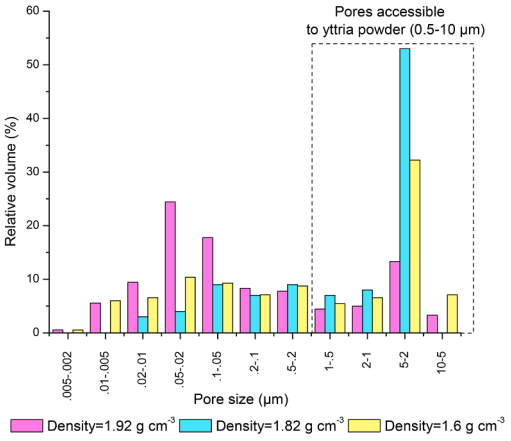

(b)

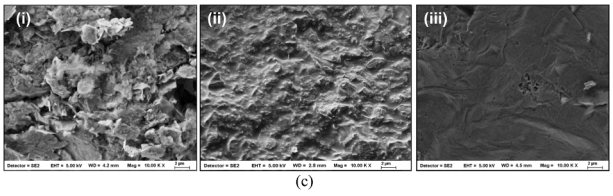

(c)

Fig. 7. (a) Particle size distribution of yttria, (b) Pore size distribution of graphite of densities 1.6 g cm^{-3}, 1.82 g cm^{-3}, 1.92 g cm^{-3} (c) Micrographs of graphite surface before coating having density (i) 1.6 g cm^{-3} (ii) 1.82 g cm^{-3} (iii) 1.92 g cm^{-3}.

0.5–10 μm range (particle size range of yttria), while graphite of density as 1.92 g cm^{-3} has a much lower volume fraction (26%) distributed over the said range of pores. As is evident from Fig. 7(b) and (c), the pores of graphite of density as 1.92 g cm^{-3} remains largely inaccessible to the yttria powder used for coating. Therefore, the yttria was mainly dissolved out from the surface of the surface, rather than the pores. Hence, the effect of resistance to diffusion is felt least in this case. On the other hand, the diffusion from pores played a significant role in the case of graphite of density as 1.82 g cm^{-3}.

In the case of graphite of density as 1.6 g cm^{-3}, the volume of pores of size more than 0.5 μm is 51%. However, the decontamination kinetics is midway between the graphite of densities as 1.92 g cm^{-3} and 1.82 g cm^{-3}. Due to easier access of the cavitation bubbles inside relatively

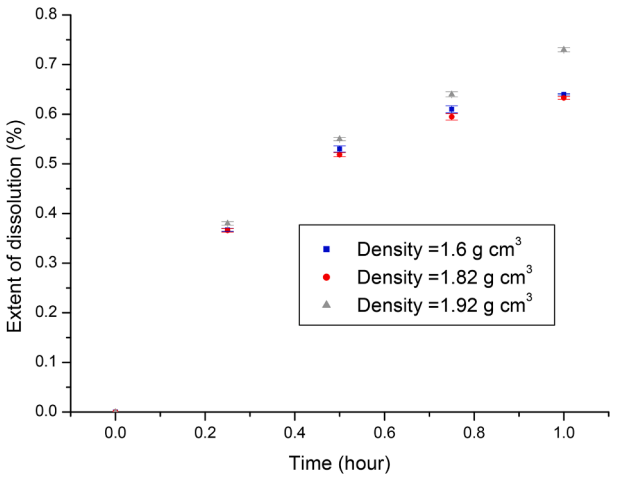

Fig. 8. Dissolution kinetics of yttria from graphite of densities as 1.6 g cm^{-3}, 1.82 g cm^{-3}, 1.92 g cm^{-3}.

large sized pores, as seen in the corresponding micrograph (Fig. 7(c)), leaching rate of yttria from graphite of density as 1.6 g cm^{-3} is faster than that from graphite of density as 1.82 g cm^{-3}. The present work is very important as it has explained the effect of particle size distribution on the dissolution characteristics in the presence of ultrasound.

4. Modelling of the dissolution kinetics

In order to scale up the process, it is important to have the kinetic data in terms of the controlling mechanism and the rate constant. A kinetic study of the dissolution process was carried out based on the well-known shrinking core model and all three possible mechanisms as film diffusion control, surface reaction control and product layer diffusion control were studied [35] for possible fitting in the current work. The shrinking core model assumes that the reaction proceeds at the solid–liquid interface which moves into the solid core, which remains unreacted. Each of the controlling mechanism based model equation can be expressed as shown in Eqs (1–3) [35]:

$$x = k_F t \text{ for film diffusion control} \quad (1)$$

$$1-(1-x)^{\frac{1}{3}} = k_S t \text{ for surface reaction control} \quad (2)$$

$$1+2(1-x)-3(1-x)^{\frac{2}{3}} = k_D t \text{ for product layer diffusion control} \quad (3)$$

where x is the reacted fraction at time t and k_F, k_S, k_D are apparent rate constants expressed as in Eqs. (4)–(6):

$$k_F = \frac{3bkC_{HNO3}}{\rho} \quad (4)$$

$$k_S = \frac{bkMC_{HNO3}}{\rho r_0} \quad (5)$$

$$k_D = \frac{2bMD_eC_{HNO3}}{\rho r_0^2} \quad (6)$$

In Eqs. (4)–(6), b is the stoichiometric coefficient; M is the molecular weight of reacted substance; ρ is the density of reacted particle; r_0 is the initial particle radius; k is the intrinsic rate constant; D_e is the effective diffusivity and C_{HNO3} is the bulk concentration of HNO_3.

The obtained results for sonication of yttria coated graphite of different densities (1.6 g cm^{-3}, 1.82 g cm^{-3}, 1.92 g cm^{-3}) at 30 kHz frequency for dissolution in 8 M HNO_3 are given in Fig. 8. It was seen that the data fitted well with the product layer diffusion control model rather than surface reaction control model. Typical regression analysis plot for graphite substrate of density 1.82 g cm^{-3} is shown in Fig. 9. The correlation coefficient is above 0.99 for the product layer diffusion control model for substrates of all the three densities of graphite, thereby clearly rejecting the other two mechanisms - film diffusion and surface reaction, based on lower values of regression coefficient as shown in Table 2. The activation energy was also calculated using the Arrhenius equation. The Arrhenius plot can be obtained from the values of reaction rate constant k_D at different temperatures. The average activation energy for the dissolution of yttria from graphite at 30 kHz was 17.8 kJ/mol for 1.82 g cm^{-3}, 14.2 kJ/mol for 1.6 g cm^{-3} and 13.6 kJ/mol for graphite of density 1.92 g cm^{-3}. Such low activation energy also points to a diffusion controlled kinetics. Higher activation energy for graphite of density 1.82 g cm^{-3} corroborates the slowest rate of dissolution, while lower activation energy for graphite of density 1.92 g cm^{-3} indicates faster kinetics. Similar product layer diffusion control mechanism was also observed in the case of uranium-coating dissolution from graphite substrate [10].

5. Conclusions

The present work established the understanding into effect of the operating parameters on the dissolution of yttria in nitric acid under the influence of ultrasound. The analysis of kinetic data showed a threefold increase in rate due to the application of ultrasound compared to dissolution under silent conditions. The operating frequency of 20 kHz was found to decontaminate the graphite surface in 30 min, best as compared to other operating frequencies, notwithstanding the erosion of the substrate. If the possible reuse of the graphite substrate is given more credence, then 30 kHz will be recommeded as the erosion of the substrate is minimum also maintaining the required level of decontamination. The dissolution rate also increased with increasing acid concentration and power intensity continuously over the entire range studied in the work. Dissolution was found to be a weak function of temperature as the change in yttrium concentration was only 5% over a temperature change of 40 °C to 60 °C. Addition of H_2O_2 to the acid leachant did not add to the dissolution rate. However, it led to higher oxidation of the substrate, thereby resulting in a net increase in weight despite surface erosion. Kinetic study established that product layer diffusion control was largely the prevailing mechanism for dissolution of yttria from graphite of all three densities. Overall, the work demonstrated the intensified decontamination of graphite substrates using ultrasound along with elucidating the product layer diffusion control as the prevailing kinetic mechanism.

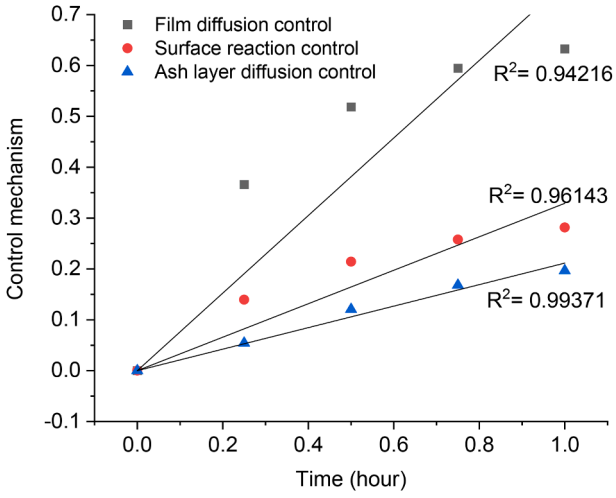

Fig. 9. Regression analysis of kinetics using shrinking core model for graphite of density 1.82 g cm^{-3} (using 8 M HNO_3 solution under 30 ± 3 kHz ultrasonic field with an acoustic intensity 8 W cm^{-2}).

Table 2
Shrinking core model equations for graphite of different densities at 30 kHz for acoustic intensity 8 W cm^{-2}.

Density of graphite (g cm^{-3})	Fitted Model equation	R^2
1.6	$1+2(1-x)-3(1-x)^{1/3} = 20.5e^{\frac{-14230}{RT}}$	0.988
1.82	$1+2(1-x)-3(1-x)^{1/3} = 20.5e^{\frac{-17820}{RT}}$	0.982
1.92	$1+2(1-x)-3(1-x)^{1/3} = 26.5e^{\frac{-13626}{RT}}$	0.993

Declaration of Competing Interest

The authors declare that they have no known competing financial interests or personal relationships that could have appeared to influence the work reported in this paper.

Acknowledgments

The authors thank R. Garg for the SEM and PSD facilities, S. K. Musharaf Ali for helping with the ICP-OES analysis facility. The authors also thank M. Mascarenhas and (Mrs) A. Sharma for their support and motivation towards this work. The work was funded by Bhabha Atomic Research Centre.

References

[1] J.J. Laidler, J.E. Battles, W.E. Miller, J.P. Ackerman, E.L. Carls, Development of pyroprocessing technology, Prog. Nucl. Energy 31 (1-2) (1997) 131–140.
[2] D. R. Harbur, J.W. Anderson, R. K. Money, Crucible coating preparation of U and Pu alloys containing Xr or HF, US Patent 3,660,075 (May 2, 1972).
[3] B. Raj, H.S. Kamath, R. Natarajan, P.R. Vasudeva Rao, A perspective on fast reactor fuel cycle in India, Prog. Nucl. Energy 47 (1-4) (2005) 369–379.
[4] Y.-L. Zhang, H.-J. Li, X.-Y. Yao, K.-Z. Li, X.-F. Qiang, Oxidation protection of C/SiC coated carbon/carbon composites with Si–Mo coating at high temperature, Corros. Sci. 53 (6) (2011) 2075–2079.
[5] X. Qiang, H. Li, Y. Zhang, Q. Fu, J. Wei, S. Tian, A modified dual-layer SiC oxidation protective coating for carbon/carbon composites prepared by one-step pack cementation, Corros. Sci. 53 (1) (2011) 523–527.
[6] F. Golestani, M. Zakeri, M. Razavi, M.R. Rahimipour, M. Shirani, Microstructureand ablative properties of Si-SiC coating prepared by spark plasma sintering, Ceram. Int. 44 (7) (2018) 8403–8408.
[7] P.V.A. Padmanabhan, S. Ramanathan, K.P. Sreekumar, R.U. Satpute, T.R.G. Kutty, M.R. Gonal, L.M. Gantayet, Synthesis of thermal spray grade yttrium oxide powder and its application for plasma spray deposition, Mater. Chem. Phys. 106 (2007) 416–421.
[8] J.W. Koger, C.E. Holcombe, J.G. Banker, Coatings on graphite crucibles used in melting uranium, Thin Solid Films 39 (1976) 297–303.
[9] C.J. Rao, A.R. Shankar, C. Mallika, U.K. Mudali, Performance evaluation of plasma sprayed yttria coatings on high density graphite for cathode processor applications, Ceram. Int. 41 (2015) 3128–3136.
[10] S. Lahiri, D. Mandal, R.L. Bhardwaj, P.R. Gogate, Intensified dissolution of uranium from graphite substrate using ultrasound, Ultrason. Sonochem. 65 (2020), 105066.
[11] P.R. Gogate, V.S. Sutkar, A.B. Pandit, Sonochemical reactors: important design and scale up considerations with a special emphasis on heterogeneous systems, Chem. Eng. J. 166 (2011) 1066–1082.
[12] A.I. Orlov, Improvement of the leaching process, Izv. Vyssh, Uchebn. Zaved Tsetn, Metall. 1 (1975) 85.
[13] M.N. Chizhikov, B.G. Novitskii, V.M. Fridman, N.N. Khavskii, Use of joint action of ultrasonic and electric field to improve leaching of metals, Sb. Mosk. Inst. Stalii Spa77 (1975) 94.
[14] P.I. Polyukhin, The use of Ultrasonics in Extractive Metallurgy Technicopy, Stonehouse, UK, 1978.
[15] B. Avvaru, S.B. Roy, S. Chowdhury, K.N. Hareendran, A.B. Pandit, Enhancement of the leaching rate of uranium in the presence of ultrasound, Ind. Eng. Chem. Res. 45 (2006) 7639.
[16] M. P. Borom, Method for rapid removal of cores made from directionally solidified eutectic and superalloy materials. US patent 4134777 (Oct 6, 1977).
[17] S. Stopic, B. Friedrich, Kinetics of yttrium dissolution from waste ceramic dust, Vojnotechnicki Glasik / Military Technical Courier 64 (2) (2016) 383–395.
[18] S. Lahiri, S. Mohapatra, K.K. Mishra, V.K. Mago, A.K. Das, L.M. Gantayet, Study on characterization of outgassing of graphite, AIP Conf. Proc. 1538 (2013) 38, https://doi.org/10.1063/1.4810029.
[19] Q. Wei, Y. Xu, Y. Wang, Textile surface functionalization by physical vapor deposition (PVD), Editor(s): Q. Wei, in Woodhead Publishing Series in Textiles, Surface Modification of Textiles, Woodhead Publishing, 2009, Pages 58-90, ISBN 9781845694197, DOI:10.1533/9781845696689.58.
[20] T.Y. Kosolapova, Carbides. Properties, Production, and Applications, first ed., Springer, US, 1971.
[21] J.B. Condon, C.E. Holcombe, Solubility of yttrium in uranium at 1700 K, J. Less Common Metals 55 (1977) 297–298.
[22] Mohammad H. Entezari, Peeter Kruus, The effect of frequency on sonochemical reactions II: temperature and Intensity effects, Ultrason. Sonochem. 3 (1) (1996) 19–24, https://doi.org/10.1016/1350-4177(95)00037-2.
[23] P.B. Subhedar, P.R. Gogate, Alkaline and ultrasound assisted alkaline pretreatment for intensification of delignification process from sustainable raw-material, Ultrason. Sonochem. 21 (2014) 216–225.
[24] Abbas Mehrdad, Robab Hashemzadeh, Hashemzadeh, Ultrasonic degradation of Rhodamine B in the presence of hydrogen peroxide and some metal oxide, Ultrason. Sonochem. 17 (1) (2010) 168–172.
[25] E.Y. Yazıcı, H. Deveci, I. Alp, T. Uslu, Generation of hydrogen peroxide and removal of cyanide from solutions using ultrasonic waves, Desalination 216 (1-3) (2007) 209–221.
[26] J. Kang, H. Hung, A. Lin, M.R. Hoffmann, Sonolytic destruction of methyl tertbutyl ether by ultrasonic irradiation: the role of O3, H2O2, frequency, and power density, Environ. Sci. Technol. 33 (1999) 3199–3205.
[27] Myunghee Lim, Younggyu Son, Jeehyeong Khim, J. Khim, The effects of hydrogen peroxide on the sonochemical degradation of phenol and bisphenol A, Ultrason. Sonochem. 21 (2014) 1976–1981.
[28] K. Bindumadhavan, S. Srivastava, I. Srivastava, Green synthesis of graphene, J. Nanosci. and Nanotechnol. 13(6) (2013) 4320-4324.
[29] Jiong Lu, Jia-xiang Yang, Junzhong Wang, Ailian Lim, Shuai Wang, Kian Ping Loh, One-pot synthesis of fluorescent carbon nanoribbons, nanoparticles and graphene by the exfoliation of graphite in ionic liquids, ACS Nano 3 (8) (2009) 2367–2375.
[30] Tapas Kuila, Partha Khanra, Nam Hoon Kim, Jae Kyoo Lim, Joong Hee Lee, Effects of sodium hydroxide on the yield and electrochemical performance of sulfonated poly(ether-ether-ketone) functionalized graphene, J. Mater. Chem. A 1 (32) (2013) 9294, https://doi.org/10.1039/c3ta11014a.
[31] Jong Hak Lee, Dong Wook Shin, Victor G. Makotchenko, Albert S. Nazarov, Vladimir E. Fedorov, Yu Hee Kim, Jae-Young Choi, Jong Min Kim, Ji-Beom Yoo, One-step exfoliation synthesis of easily soluble graphite and transparent conducting graphene sheets, Adv. Mater. 21 (2009) 4383–4387.
[32] K. Rao, J. Senthilnathan, Y.F. Liu, M. Yoshimura, Role of peroxide ions in formation of graphene nanosheets by electrochemical exfoliation of graphite, Sci Rep 4 (2014) 4237, https://doi.org/10.1038/srep04237.
[33] Konstantinos Spyrou, Longtian Kang, Evmorfia K. Diamanti, Regis Y. Gengler, Dimitrios Gournis, Maurizio Prato, Petra Rudolf, A novel route towards high quality fullerene-pillared graphene, Carbon 61 (2013) 313–320.
[34] S. Pruvost, C. Herold, A. Herold, P. Lagrange, Co-intercalation into graphite of lithium and sodium with an alkaline earth metal, Carbon 42 (2004) 1825–1831.
[35] O. Levenspiel, Chemical Reaction Engineering, Wiley, New York, 1972.